Towards Prediction of Aircraft Spin

Kyle D. Squires
Arizona State University

James R. Forsythe
United States Air Force Academy

Ken E. Wurtzler, William Z. Strang, Robert F. Tomaro
Cobalt Solutions, LLC

Matthew J. Grismer
Air Force Research Laboratory/Air Vehicles Directorate

Philippe R. Spalart
Boeing Commercial Airplanes

Abstract

A new approach for prediction of unsteady turbulent flows is being developed and applied in this research. The long-term aim of this work is to develop a method for prediction of massively separated flows. The initial effort is focused on development of a Computational Fluid Dynamics (CFD) tool for prediction of aircraft spin. The simulation technique is known as Detached-Eddy Simulation (DES) and is being used to solve the compressible Navier-Stokes equations. Research has focused on both fundamental aspects of the technique and practical applications of importance to current DoD needs. Research on fundamental issues is concerned with prediction of the flow around simplified models of an aircraft forebody in crossflow. Accurate simulation of the flow around the forebody is crucial to prediction of spin characteristics. The aim of these studies has been to assess the accuracy of DES for prediction of the unsteady flow and forces on the body at flight Reynolds numbers and to investigate aspects of the turbulence model relevant to predicting boundary layer separation. The cross-section of the geometry is a rounded-corner square with its spanwise axis normal to the freestream. DES predictions show that time histories of the forces acting on the body exhibit a complex modulation associated with vortex shedding. High Reynolds number predictions of the pressure distribution and forces on the body are in good agreement with measurements, more accurate than solutions obtained from unsteady Reynolds-averaged Navier-Stokes (RANS) calculations and Monotone Integrated Large Eddy Simulation.

In the second phase of the work, DES is being used to predict the flow around an F-15E at 65° angle-of-attack. The goal is to assess DES predictions against both measurements and numerical models currently used in engineering practice. Solutions are obtained on unstructured grids comprised of 5.9 million cells (prisms in the boundary layers, tetrahedra in other regions). DES predictions of forces and moments compare favorably to flight test data and are more accurate than solutions obtained from RANS calculations. The computational

cost of the DES was essentially the same as that of unsteady RANS. All of the calculations described above are performed on structured and unstructured grids using a flow solver – Cobalt_{60} – which uses Message Passing Interface for parallel solution. Calculations have been performed on a variety of HPC machines. Depending on the problem size, solutions are obtained on as many as 512 processors, providing full aircraft, unsteady solutions in approximately one day.

Introduction

Most of the flow fields encountered in DoD applications occur within and around complex devices and at speeds for which the underlying state of the fluid motion is turbulent. While Computational Fluid Dynamics (CFD) is gaining increased prominence as a useful approach to analyze and ultimately design configurations, efficient and accurate solutions require substantial effort and expertise in several areas. Geometry description and grid generation, numerical solution of the Navier-Stokes equations, and efficient post-processing are all key elements.

While advances have taken place in areas such as grid generation and fast algorithms for solution of systems of equations, CFD has remained limited as a reliable tool for prediction of inherently unsteady flows at flight Reynolds numbers. Current engineering approaches to prediction of unsteady flows are based on solution of the Reynolds-averaged Navier-Stokes (RANS) equations. The turbulence models employed in RANS methods necessarily model the entire spectrum of turbulent motions. While often adequate in steady flows with no regions of reversed flow, or possibly exhibiting shallow separations, it appears inevitable that RANS turbulence models are unable to accurately predict phenomena dominating flows characterized by massive separations. Unsteady massively separated flows are characterized by geometry-dependent and three-dimensional turbulent eddies. These eddies, arguably, are what defeats RANS turbulence models, of any complexity.

To overcome the deficiencies of RANS models for predicting massively separated flows, Spalart *et al.* [1] proposed Detached-Eddy Simulation (DES) with the objective of developing a numerically feasible and accurate approach combining the most favorable elements of RANS models and Large Eddy Simulation (LES). The primary advantage of DES is that it can be applied at high Reynolds numbers as can Reynolds-averaged techniques, but also resolves geometry-dependent, unsteady three-dimensional turbulent motions as in LES. DES predictions to date have been favorable, forming one of the motivations for this research. The specific aims of this work are to apply and assess DES, consistent with the long-term goal of developing a CFD tool for analysis and prediction of aircraft spin. The first phase of the work has focused on fundamental aspects of the technique relevant to aircraft spin, the second phase of the work is an application of the method to prediction of the time-dependent flow around full aircraft. The third phase of the work is development, testing, and application of moving grid capability for spin prediction of an isolated forebody and the F-15E.

The flow considered in the first phase of the work is the massive separation around a forebody with the freestream at angle of attack to the long axis of the body. The forebody plays a major role in determining the stability characteristics and spin modes of modern aircraft. Vortical flows, crossflow separations, and sensitivity of forces and moments to Reynolds

number lead to complex effects that are difficult to capture using current simulation techniques. The aim has been to evaluate predictions of the unsteady flow around the forebody via comparison against unsteady RANS predictions and the experimental measurements of Polhamus *et al.* [2]. Also important has been to gauge the stability of DES predictions to changes in grid refinement and the dimension of the spanwise coordinate. In the second phase of the work, the unsteady flow around a full aircraft – an F-15E at 65° angle of attack – is computed.

For both studies, high performance computation is essential. In this work, solutions of the compressible Navier-Stokes equations are obtained using Cobalt_{60} (Strang *et al.* [3]). In Cobalt_{60}, solutions of the compressible Navier-Stokes equations are obtained on unstructured grids. The numerical method is based on a finite-volume approach and is second-order accurate in space and time. The method is point-implicit and permits CFL numbers as large as one million for steady-state computations (Tomaro *et al.* [4]). Turbulence-resolving simulations are necessarily time dependent and for DES calculations the code is run in a time-accurate fashion (as well as for the unsteady RANS predictions presented below). Calculations using Cobalt_{60} are performed in parallel using the Message Passing Interface (see Grismer *et al.* [5]). The parallel performance of the code is excellent and a discussion is presented below on the rapid turnaround possible for DES predictions on unstructured grids of full aircraft.

The governing equations and turbulence model used in this research are presented in the next section. Following is a summary of the flow conditions considered for the forebody in crossflow and then the F-15E. Results from the simulations are presented and, finally, a summary of the work and some future directions are discussed.

Numerical Approach

Governing equations and turbulence models

The Navier-Stokes equations are solved in an inertial reference frame and can be written in integral form as,

$$\frac{\partial}{\partial t}\iiint_{\mathcal{V}} Q\, d\mathcal{V} \;+\; \iint_{\mathcal{S}} (f\hat{\imath} \;+\; g\hat{\jmath} \;+\; h\hat{k}) \;\cdot\; \hat{n}\, d\mathcal{S} \quad = \quad \iint_{\mathcal{S}} (r\hat{\imath} \;+\; s\hat{\jmath} \;+\; t\hat{k}) \;\cdot\; \hat{n}\, d\mathcal{S}$$

where:

$$Q = \begin{bmatrix} \rho \\ \rho u \\ \rho v \\ \rho w \\ \rho e \end{bmatrix} \quad f = \begin{bmatrix} \rho u \\ \rho u^2 + p \\ \rho uv \\ \rho uw \\ u(\rho e + p) \end{bmatrix} \quad g = \begin{bmatrix} \rho v \\ \rho uv \\ \rho v^2 + p \\ \rho vw \\ v(\rho e + p) \end{bmatrix} \quad h = \begin{bmatrix} \rho w \\ \rho uw \\ \rho vw \\ \rho w^2 + p \\ w(\rho e + p) \end{bmatrix}$$

$$r = \begin{bmatrix} 0 \\ \tau_{xx} \\ \tau_{xy} \\ \tau_{xz} \\ a \end{bmatrix} \quad s = \begin{bmatrix} 0 \\ \tau_{xy} \\ \tau_{yy} \\ \tau_{yz} \\ b \end{bmatrix} \quad t = \begin{bmatrix} 0 \\ \tau_{xz} \\ \tau_{yz} \\ \tau_{zz} \\ c \end{bmatrix}$$

In the above, $a = u\tau_{xx} + v\tau_{xy} + w\tau_{xz} + kT_x$, $b = u\tau_{xy} + v\tau_{yy} + w\tau_{yz} + kT_y$, and $c = u\tau_{xz} + v\tau_{yz} + w\tau_{zz} + kT_z$. A fluid element volume over which the equations are enforced is denoted $\mathcal{V}$; the bounding surface as $\mathcal{S}$ with outward-pointing unit normal $\hat{n}$. The Cartesian unit vectors are $\hat{\imath}$, $\hat{\jmath}$, and $\hat{k}$; ρ is the density; p is the pressure; u, v, and w are the velocity components; e is the specific energy per unit volume; T is the temperature; k is the thermal conductivity; and τ_{xx}, τ_{yy}, τ_{zz}, τ_{xy}, τ_{xz}, and τ_{yz} are the viscous stress tensor components. The ideal gas law closes the system of equations and the entire equation set is non-dimensionalized by freestream density and speed of sound.

Integrating the equations around finite volumes in the domain leads to the semi-discrete form for the system,

$$\mathcal{V}_i \frac{dQ_i}{dt} + \sum_{M=1}^{N_i} (f^M \hat{\imath} + g^M \hat{\jmath} + h^M \hat{k}) \cdot \hat{n}^M \mathcal{S}^M = \sum_{M=1}^{N_i} (r^M \hat{\imath} + s^M \hat{\jmath} + t^M \hat{k}) \cdot \hat{n}^M \mathcal{S}^M$$

where the subscripted i and superscripted M denote quantities for the i^{th} cell and the M^{th} face of cell i, respectively, and N_i is the number of faces bounding cell i. The equations above can be solved on arbitrary cell types in Cobalt$_{60}$. For the current study both structured and unstructured grids are used. The unstructured grids contain a combination of tetrahedra and prisms, while the structured grids are comprised of hexahedra. Prisms are used in the boundary layer in order to reduce the number of cells as well as to improve the boundary layer computation. Boundary-layer grids comprised of tetrahedra often possess high aspect ratios and can be strongly non-orthogonal. This presents problems in calculation of the divergence of the gradient (Forsythe *et al.* [6]). Prisms are more orthogonal and place less burden on the solver.

For simulation of turbulent flows the governing equations are suitably averaged, yielding turbulent stresses that require a model. A Boussinesq approximation is invoked in the momentum equations and the turbulent eddy viscosity (μ_t) is used to relate the stresses to the strain rate. The turbulent heat flux is also modeled using a gradient-transport hypothesis, requiring specification of a turbulent thermal conductivity k_t. Reynolds analogy is applied and the turbulent heat flux is modeled using a constant turbulent Prandtl number of 0.9. Using turbulent eddy viscosity and turbulent conductivity, the variable μ is replaced by $(\mu + \mu_t)$ and k is replaced by $(k + k_t)$ in the governing equations.

A Newton method is used in solution of the system of equations. In the calculations presented below, a minimum of two Newton sub-iterations were used for all time accurate cases, which roughly doubles the cost of each step compared to a steady-state calculation, but is necessary to ensure time accuracy (steady state calculations are performed with zero or one subiteration). In addition, to obtain sufficient samples in the averages, statistics were acquired over a minimum of 100 time units (L/V_∞). With the (dimensionless) timestep usually set to 0.01, this required 10,000 iterations. Steady state calculations require on average about 2,000 iterations (c.f., Figures 11 through 13).

Spalart-Allmaras turbulence model

The Spalart-Allmaras (SA) one-equation model (Spalart and Allmaras [7]) solves a single partial differential equation for a working variable $\widetilde{\nu}$ which is related to the turbulent viscosity. The differential equation is derived by "using empiricism and arguments of dimensional

analysis, Galilean invariance and selected dependence on the molecular viscosity." The model includes a wall destruction term that reduces the turbulent viscosity in the laminar sublayer and trip terms that provide for a smooth transition from laminar to turbulent behavior (note that the trip term is not used in the calculations presented in this manuscript). The model takes the form,

$$\frac{D\widetilde{\nu}}{Dt} = c_{b1}\widetilde{S}\,\widetilde{\nu} - c_{w1}f_w\left[\frac{\widetilde{\nu}}{d}\right]^2 + \frac{1}{\sigma}\left[\nabla\cdot\left(\left(\nu+\widetilde{\nu}\right)\nabla\widetilde{\nu}\right) + c_{b2}\left(\nabla\widetilde{\nu}\right)^2\right] .$$

The turbulent viscosity is obtained from,

$$\nu_t = \widetilde{\nu}\,f_{v1}\,, \qquad f_{v1} = \frac{\chi^3}{\chi^3 + c_{v1}^3}\,, \qquad \chi \equiv \frac{\widetilde{\nu}}{\nu}$$

where S is the magnitude of the vorticity, and the modified vorticity is,

$$\widetilde{S} \equiv S + \frac{\widetilde{\nu}}{\kappa^2 d^2} f_{v2}\,, \qquad f_{v2} = 1 - \frac{\chi}{1+\chi\,f_{v1}}$$

where d is the distance to the closest wall. The wall destruction function f_w is,

$$f_w = g\left[\frac{1+c_{w3}^6}{g^6+c_{w3}^6}\right]^{\frac{1}{6}}$$

$$g = r + c_{w2}(r^6 - r)\,, \qquad r \equiv \frac{\widetilde{\nu}}{\widetilde{S}\kappa^2 d^2}$$

The model coefficients are,

$$\begin{array}{ccc} c_{b1} = 0.1355 & \sigma = \frac{2}{3} & c_{b2} = 0.622 \\ \kappa = 0.41 & c_{w1} = c_{b1}/\kappa^2 + (1+c_{b2})/\sigma & c_{w2} = 0.3 \\ c_{w3} = 2 & c_{v1} = 7.1 & \end{array}$$

Detached-Eddy Simulation

Detached-Eddy Simulation is based on a simple modification to the Spalart-Allmaras model summarized above. Note that in the SA model, the wall destruction term is proportional to $(\widetilde{\nu}/d)^2$, where d is the distance to the closest wall. When this term is balanced with the production term, the eddy viscosity becomes $\widetilde{\nu} \propto Sd^2$, where S is the local strain rate. The Smagorinsky subgrid-scale (SGS) model varies its turbulent viscosity with the local strain rate, and the filter width (usually the grid spacing), Δ, i.e. $\nu_{SGS} \propto S\Delta^2$. Replacing d by Δ in the wall destruction term, therefore, transforms the SA model to a subgrid closure and both RANS and LES behavior can be obtained by re-defining d as:

$$\widetilde{d} = \min\left(d, C_{DES}\Delta\right) .$$

When $d \ll \Delta$, the model reduces to its RANS form. When $d \gg \Delta$, the closure behaves as a subgrid-scale model. Therefore, the model can be "switched" to an "LES mode" by

locally refining the grid. In an attached boundary layer, a RANS simulation will have highly stretched grids in the streamwise direction. To retain RANS behavior in this case Δ is taken as the largest spacing along any direction ($\Delta = \max(\Delta x, \Delta y, \Delta z)$). To compute the modified wall distance $\widetilde{d}$ for DES, the longest distance between any given cell center and its neighbors is used. Following Shur *et al.* [8], the model constant $C_{DES} = 0.65$ was used in the calculations.

Results

Forebody in crossflow

A cross-section of the rounded-corner square is shown in Figure 1. The corner radius is equal to 1/4 of the width/height ("diameter") of the forebody. The configuration under consideration is the flow at 10° incidence and oriented normal to the spanwise axis (the coordinate out of the page in the figure). Experimental measurements of the configuration shown in Figure 1 are available for several Reynolds numbers and also over a wide range of incidence angles (Polhamus *et al.* [2]). Measurements show a strong sensitivity of the streamwise and lateral forces with Reynolds number, with a reversal of the lateral force occurring for Reynolds numbers around 500,000.

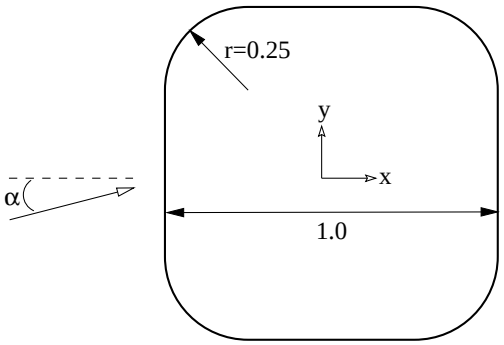

Figure 1: Forebody cross section. The corner radius is 1/4 of the total length ("diameter") of the side.

The spanwise coordinate of the flow is statistically homogeneous with periodic end conditions employed in the calculations. Simulations have been performed at sub- and super-critical Reynolds numbers for which changes in boundary layer separation leads to a reversal of the lateral force. DES predictions are assessed for a modest range of grid refinement, in calculations with a doubling of the spanwise period, and also using simulations performed without the model. These runs without a turbulence model are denoted as MILES (Monotone Integrated Large Eddy Simulation) to provide a link with relevant literature, although no detailed investigations were undertaken to evaluate the numerical dissipation in the current calculations and its role as an SGS model, and the numerical schemes are not monotone in a strict sense. The reader is referred to the paper of Fureby and Grinstein [9] for an overview of the MILES approach.

Results are presented in this section for flows in the super-critical regime, computed at a Reynolds number of 800,000. A fully turbulent solution is established by introducing

Case	Model	Grid Size	L_z	$\langle C_x \rangle$	$\langle C_y \rangle$
1	DES	$100 \times 149 \times 151$	3	0.57	0.92
2	DES	$100 \times 149 \times 301$	6	0.56	0.99
3	DES	$150 \times 200 \times 151$	3	0.51	0.96
4	DES	$120 \times 149 \times 151$ (pad)	3	0.49	0.95
5	DES	uns - 3.55×10^6 cells	3	0.43	0.83
6	MILES	$120 \times 149 \times 151$ (pad)	3	0.76	0.63
7	URANS	200×400	-	0.75	0.87
	Exp.	-	-	0.4	0.9

Table 1: Parameters for solution of the super-critical flow ($Re = 800,000$) around the rounded-corner square. "uns" for Case 5 denotes use of an unstructured grid; "pad" denotes calculations performed on the larger domains; $\langle C_x \rangle$ and $\langle C_y \rangle$ are the streamwise and lateral force coefficients.

a small level of eddy viscosity at the inflow boundary (three times the molecular value), effectively igniting the model as the fluid enters the boundary layers. Turbulent boundary layer separation occurs near the rear of the body with a chaotic and three-dimensional structure characterizing the wake.

The simulation parameters are summarized in Table 1, identifying the simulation technique, grid size, spanwise dimension (L_z), and the resulting time-averages of the axial and normal forces. The experimental measurements of Polhamus *et al.* [2] are also included for comparison.

The structured grids used for the forebody were generated using the control technique of Hsu and Lee [10]. This approach permits control of the mesh spacing to the first point nearest the boundary (within one wall unit near solid boundaries), control over grid spacings tangential to the boundary, and also maintains orthogonality of the grid at all boundaries.

As summarized in Table 1, the baseline cases are comprised of grids having approximately 2.25 million cells (100×149 points in the x-y plane, shown in Figure 2). The farfield boundaries for the first three cases were located approximately 5 "diameters" from the body. For the next three cases the grid was extended to 20 "diameters" away the body to examine domain-size influences. The effect of the spanwise period and influence of the periodic end conditions employed in this direction was examined in simulations performed on domains with a doubling of the spanwise coordinate (Case 2) compared to the baseline case (Case 1). A two-dimensional unsteady RANS calculation using the Spalart-Allmaras model is also summarized in the table.

Shown in Figure 3 is a snapshot of the vorticity field (colored by pressure) from Case 2. The visualization shows the separation (of fully turbulent boundary layers) at the rear of the body along the upper and lower flat surfaces. DES is well suited for flows in which rapid new instabilities will dominate the separated region, lessening errors from the lack of structural content in the detaching boundary layers. Figure 3 shows the RANS boundary layers rapidly break down as the flow separates and the wake develops chaotic and three dimensional motions. The figure also shows alternate vortex shedding along the spanwise coordinate occurring sometimes near the top surface, and at other positions near the bottom.

This effect is probably at least partly responsible for the frequency modulation observed in the force histories (Figure 4).

The unsteady nature of the flow has a strong effect on the streamwise and lateral force coefficients shown in Figure 4. A transient of roughly 20 non-dimensional time units has been excluded from the time histories in the figure. A strong modulation is apparent in the side force, similar to related studies of vortex shedding from cylinders and other bluff bodies (e.g., see Travin *et al.* [11]). This modulation is not predicted in unsteady RANS calculations (not shown in the figure) and is an intrinsic feature of the chaotic, unsteady flow. DES calculations on domains in which the spanwise coordinate L_z was 1.5 diameters damped these modulations and suppressed three-dimensional effects, yielding two-dimensional solutions and resulting in large over-predictions of the axial force.

Pressure coefficients around the body are shown in Figure 5. The angle θ is measured clockwise from the front-center of the forebody. Note that on the smaller domains (Cases 1-3 in Table 1), the stagnation C_p is too large. Comparing the effect of the domain size (Case 1 and Case 4) shows a reduction in the axial force coefficient on the larger domain, closer to the measured value of about 0.4. Along the rear vertical surface of the body (in the vicinity of $\theta = 0$ in Figure 5) the URANS pressure distribution is far from the measured values, resulting in a large streamwise force (c.f., Table 1) as similarly observed in other URANS predictions of bluff-body flows. The MILES calculation, performed without a turbulence model, improves the prediction of the rear-surface pressures. However, the peak suction around the upper front corner ($\theta = 135°$) in the MILES is poorly predicted because the (laminar) boundary layers separate, rather than remaining attached. DES predictions on the unstructured grid (also on the larger domain) yield a streamwise force that is closest to the measured value. Table 1 also shows that DES predictions of the lateral force coefficient $\langle C_y \rangle$ are in general not far from the measurements reported by Polhamus *et al.* [2]. The lateral force prediction in the MILES case provides an illustration of the significant error that can arise due to the boundary layer treatment in this technique. Accurate prediction of boundary layer growth and separation in MILES requires the boundary layer grid be fine enough to resolve the small near-wall turbulent structures (as would also be required in whole-domain LES with an explicit SGS model). In practice, however, the grids are not sufficiently fine for large Reynolds numbers because of the high computational cost. The resulting boundary layer is absent of turbulent structures and is essentially laminar.

Flow around and F-15E at $\alpha = 65°$

Computations were performed of the flow over an F-15E at $\alpha = 65°$ and zero sideslip. Boeing provided the authors with a stability and control database for the F-15E that was developed from a comprehensive spin testing program (courtesy of Ken Walck and Glen Peters of Boeing Military). Two stable spin conditions were detailed, including data for symmetric and asymmetric fuel loads. The aircraft with symmetric loading maintains a stable spin at 65° angle of attack. Prior to computing the actual spin using rigid body moving grids, the performance of the computational model was investigated at the same fixed angle of attack as for the stable spins. All computations were made matching the flight test conditions at a Mach number of 0.3 and standard day 30,000 feet. This resulted in a chord based Reynolds number of 13.6 million.

A grid for half of the F-15E was created using VGRIDns (Pirzadeh [12]), and is shown in Figure 7. The original grid consisted of 7.9 million tetrahedral cells. Using a grid utility developed by the Air Force Research Laboratories Air Vehicles Directorate, nine layers in the boundary layer were combined into prisms, dropping the total number of cells to 5.9 million. The distance from solid surfaces to the first cell center normal to the wall was constant, resulting in an average distance in wall units (y_1^+) of 0.7. Cell growth in the wall-normal direction was specified using a geometric stretching factor of 1.3. There were approximately 160,000 faces on the surface of the aircraft with only a few hundred cells on the outer boundary, as seen in Figure 6. Note that a structured multiblock grid would be less 'efficient', having the same number of cells on the outer boundary as on the surface. A chimera grid could eliminate this deficiency, but would introduce interpolation error. Another advantage of an unstructured grid in DES is that the tetrahedra outside the boundary layer are nearly isotropic, such cell-types sometimes difficult to achieve using a structured approach. Isotropic cells ensure the lowest value of Δ for a given cell volume, lowering the eddy viscosity and allowing more turbulence to be resolved rather than modeled. Also, since the orientation of turbulent structures are not necessarily known *a priori*, isotropic cells are a logical approach to representing the eddies.

Steady-state RANS calculations were first performed using the Spalart-Allmaras (SA) model. These simulations are computationally efficient since it is possible to take advantage of the implicit nature in the numerical method, the steady-state computations were performed using a CFL of one million. An unsteady RANS (URANS) calculation was not made based on experience with URANS on the F-16 in which the time-accurate URANS using the SA model evolved to essentially a steady solution (c.f., Figure 8). Figure 8 compares a DES and URANS (SA) solution at 45° angle of attack on the same grid (3.1 million cells) and using the same timestep in each calculation. The SA model yielded nearly a steady solution, with oscillations about the mean values of the lift and drag less than 1%. DES, on the other hand, exhibited fairly large levels of unsteadiness even on this coarse grid, with a particularly energetic vortex burst. DES calculations were then performed on the F-15E using non-dimensional timesteps of 0.01 and 0.02 (made dimensionless using the mean chord and freestream velocity).

Side by side comparisons of DES and RANS predictions across the symmetry plane are shown in Figures 9 and 10. The contours and isosurfaces of vorticity illustrate the capability of DES in "LES mode" resolving the unsteady, geometry-dependent flow features. Force histories of C_L, C_D, and C_M for the two simulation techniques are next compared to the Boeing database in Figures 11 through 13. The SA predictions are accurate, an interesting finding given the model is applied in a flow far from its calibration range. The largest discrepancy is in the moment coefficient, which is over-predicted (in a negative sense) by 10%. The lift and drag coefficients are over-predicted by 9% and 7% respectively. DES predictions of these quantities are all within 4% for both timesteps. The expected accuracy of the Boeing database for this angle of attack is anticipated to be around 5% (Peters, private communication) and, therefore, the DES predictions are certainly satisfactory. Any further improvements would be within the estimated error and would not necessarily indicate a more accurate method.

To examine the source of the differences between the RANS and DES results, the pressure coefficient from the (steady state) RANS is compared to the time average of the DES

predictions in Figure 14. As evident from the figure, DES yields a relatively flat profile in C_p that is the norm on a wing with separation, while the RANS predicts a more varied pressure distribution. Overall, however, the RANS prediction of the F-15E is relatively accurate, better than obtained in solutions of canonical flows such as that around a two-dimensional NACA airfoil at angle of attack (Shur *et al.* [8]). The relatively strong coherent vortex shedding around two-dimensional shapes such as an airfoil or cylinder remains problematic for RANS due to the inability of these models to accurately account for the modulation in the shedding (c.f., Figure 4). The flow over the F-15E appears not as strongly dominated by coherent shedding over a limited frequency band, lessening the burden on RANS models to account for strong modulation in the forces.

Computational Aspects

In the current study, the computational cost of the time-accurate calculations is roughly an order of magnitude greater than a steady-state run. The unsteady RANS calculations carry the same cost as DES if the grid and time step are the same and if the sampling period for calculation of averaged quantities is fixed. The current calculations, although not yet demonstrating grid-convergent solutions, suggest that DES exhibits improved predictions on a grid originally designed for RANS. Although a factor of ten increase in cost may seem large, if Moore's law continues to hold, this factor of ten will be surpassed in less than three and a half years. Thus, facilities that can currently support steady RANS calculations on full aircraft should be able to accommodate DES runs on at least coarse grids.

Initial forebody calculations were performed on the Air Force Academy's Linux cluster, *blackbird* – a 64 processor cluster using Pentium IIIs and 100Btx switched ethernet. Calculations on the coarse grid (2 million cells) required approximately one week to run 100 time units. Subsequent simulations have been performed at NAVO's T3E - *seymour*, or Maui HPC's IBM SP3 - *tempest*. A complete DES run (100 time units, 10,000 iterations, 3.1 million cells) on the F-16 was computed on *tempest* using 432 processors, and was completed in 12.5 hours. The F-15E runs (5.9 million cells) were computed using 256 processors and required 2-3 days. For the DES runs, the F-15E grid was mirrored about the symmetry plane, resulting in 11.8 million cells. These runs required approximately four days on 256 processors and were computed using a timestep of 0.01. Figures 11 through 13 suggest that a timestep of 0.02 would be sufficient, cutting the computation time in half.

Given the processing power of HPC and the parallel efficiency of Cobalt$_{60}$, the bottleneck could have been the generation of the grid. Unstructured grids used in the current work reduced the time needed for grid generation compared to what can be required for generation of structured meshes. Grids were made using both VGRIDns (Pirzadeh [12]) and Gridgen (Steinbrenner *et al.* [13]), the task requiring about one week for each grid. Structured and unstructured grids were created for the forebody, requiring on average less than one day (following development of the elliptic solver). The shorter time requirement due to the relative simplicity of the geometry.

Summary

For the forebody-in-crossflow, DES predictions are fairly robust, in general tending towards experimental measurements with grid refinement, for example. The complex shedding process and modulation in the forces appear to be represented reasonably well. The chaotic nature of the solution complicates comparison to experimental measurements and highlights the difficulty in 'refined' evaluation of simulation against experiments (see Spalart [14]). In the DES solutions presented here, the attached boundary layers were fully turbulent. While a fully turbulent computation seems sufficient for the case considered, in other regimes (e.g., at lower Reynolds numbers) there can be substantial regions of laminar flow on the body and a prediction of boundary layer transition is required. Details of the separation process and transition to turbulence are often inter-mingled and continue to strongly challenge current modeling approaches. To date, efforts at predicting sub-critical flows have not been as successful as the fully turbulent runs presented in this manuscript.

For the F-15E, the present DES calculations are probably one of the first applications of a turbulence-resolving technique to full aircraft at flight Reynolds numbers in which turbulent boundary layers on the vehicle were represented without recourse to wall functions (i.e., with grid spacings within one viscous unit at the wall). Calculations on finer grids are needed to increase confidence in the method, though the present results are encouraging. Incorporation of additional effects such as rigid-body motion can also be considered and explored.

Combining the time for grid generation and solution, a DES calculation could be made within two weeks, given the performance of the HPC machines. For a small linux cluster such as that at the USAF Academy, the computations themselves comprise the bottleneck, requiring from a week to a month for a single aircraft. In six years, if Moore's law continues, a linux cluster such as *blackbird* could be 16 times more powerful, in turn producing a DES solution in 12 hours to two days. HPC, meanwhile, will also see its capacity increase by approximately 16 times, allowing rapid solutions for grids nearing 200 million cells. As grids are made more dense, the fidelity of the DES solutions will improve for the current simulation (static aircraft). Alternatively, increased computing capacity will enable the incorporation of additional physical effects into the modeling.

Acknowledgments

The first author gratefully acknowledges the support of AFOSR Grant F49620-00-1-0050 (Program Manager: Dr. Tom Beutner). The authors are also grateful for the assistance of Dr. Glen Peters, Dr. Ken Walck, and Dr. Walt Labozzetta of Boeing Military, who provided the stability and control database and the F-15E geometry. Mr. Matthieu Chapelet and Cadet Kory Klismith have assisted with grid generation and post-processing. Cadet Warren Carroll and Cadet Alan VantLand aided in post-processing the F-15E results. Finally, the project would not have been possible without the support and cpu hours at NAVO MSRC and Maui HPCC.

References

[1] Spalart, P.R., Jou, W-H., Strelets, M., and Allmaras, S.R., "Comments on the Feasibility of LES for Wings, and on a Hybrid RANS/LES Approach" *Advances in DNS/LES, 1st AFOSR Int. Conf. on DNS/LES*, Aug. 4-8, 1997, Greyden Press, Columbus OH.

[2] Polhamus, E.C., Geller, E.W. and Grunwald, K.J., "Pressure and Force Characteristics of Noncircular Cylinders as Affected by Reynolds Number with a Method Included for Determining the Potential Flow about Arbitrary Shapes", NASA TR R-46, 1959.

[3] Strang, W.Z., Tomaro, R.F, Grismer, M.J., "The Defining Methods of Cobalt$_{60}$: a Parallel, Implicit, Unstructured Euler/Navier-Stokes Flow Solver," *AIAA 99-0786,* January 1999.

[4] Tomaro, R.F., Strang, W.Z., and Sankar, L.N., "An Implicit Algorithm for Solving Time Dependent Flows on Unstructured Grids," *AIAA 97-0333*, January 1997.

[5] Grismer, M.J., Strang, W.Z., Tomaro, R.F. and Witzeman, F.C., "Cobalt: A Parallel, Implicit, Unstructured Euler/Navier-Stokes Solver," *Advances in Engineering Software*, **29**, pp. 365-373, 1998.

[6] Forsythe, J.R., Strang, W.Z. and Hoffmann, K.A., "Validation of Several Reynolds-Averaged Turbulence Models in a 3-D Unstructured Grid Code," *AIAA 00-2552,* June 2000.

[7] Spalart, P.R. and Allmaras, S.R. "A One-Equation Turbulence Model for Aerodynamic Flows", *La Recherche Aérospatiale*, 1994, **1**, p. 5.

[8] Shur, M., Spalart, P. R., Strelets, M., and Travin, A, "Detached-Eddy Simulation of an Airfoil at High Angle of Attack, 4th Int. Symp. Eng. Turb. Modelling and Measurements, Corsica, May 24-26, 1999.

[9] Fureby, C. and Grinstein, F.F., "Monotonically integrated large eddy simulation of free shear flows", *AIAA J.*, **37**, pp. 544-556, 1999.

[10] Hsu, K. and Lee, S.L., "A Numerical Technique for Two-Dimensional Grid Generation with Grid Control at All of the Boundaries", *Journal of Computational Physics*, 1991, **11**, pp. 451-469.

[11] Travin, A., Shur, M., Strelets, M. and Spalart, P., "Detached-Eddy Simulations past a Circular Cylinder", *Flow, Turbulence and Combustion*, 2001.

[12] Pirzadeh, S., "Three-dimensional Unstructured Viscous Grids by the Advancing Layers Method," *AIAA Journal*, 1996, **34**, pp. 43-49.

[13] Steinbrenner, J., Wyman, N., Chawner, J., "Development and Implementation of Gridgen's Hyperbolic PDE and Extrusion Methods," *AIAA 00-0679*, January 2000.

[14] Spalart, P. R., "Strategies for Turbulence Modelling and Simulations", *Int. J. Heat Fluid Flow*, **21**, 252-263, 2000.

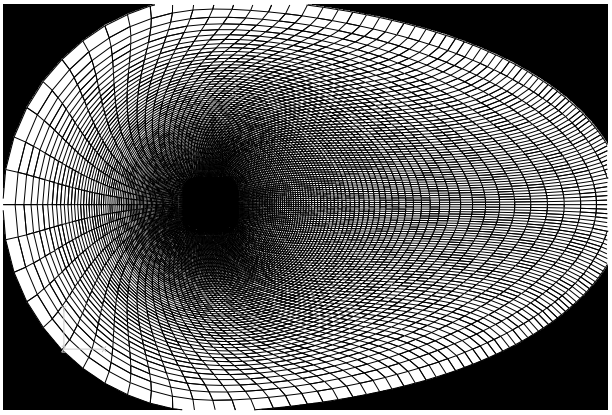

Figure 2: Cross-section (in the x-y plane) of the grid. 100×149 points.

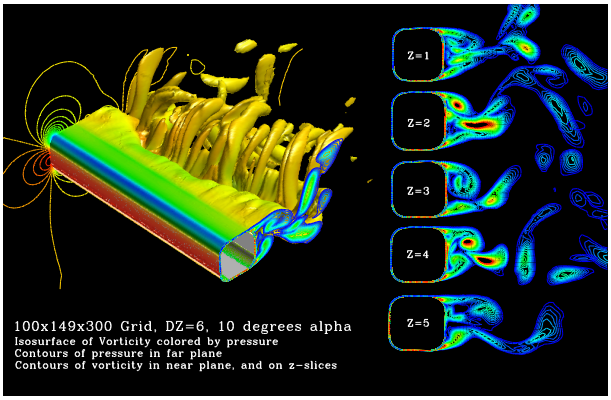

Figure 3: Instantaneous vorticity field (colored by pressure) for Case 2.

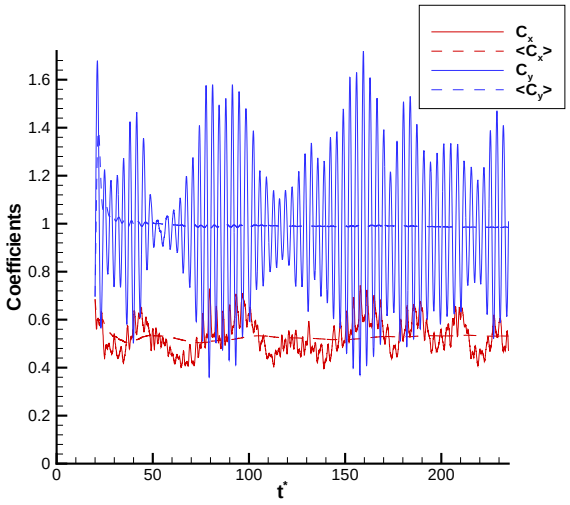

Figure 4: Time history of the streamwise (C_x) and lateral (C_y) forces for Case 2.

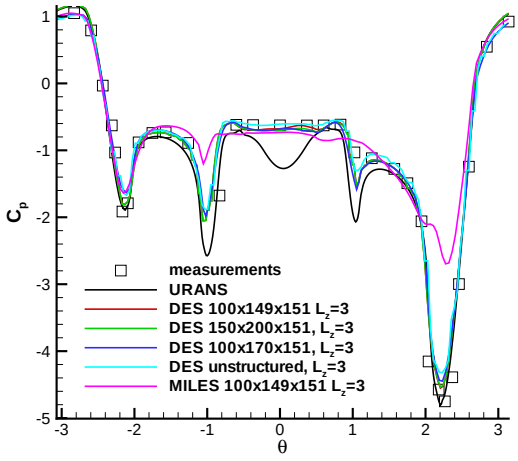

Figure 5: Pressure coefficient from various runs.

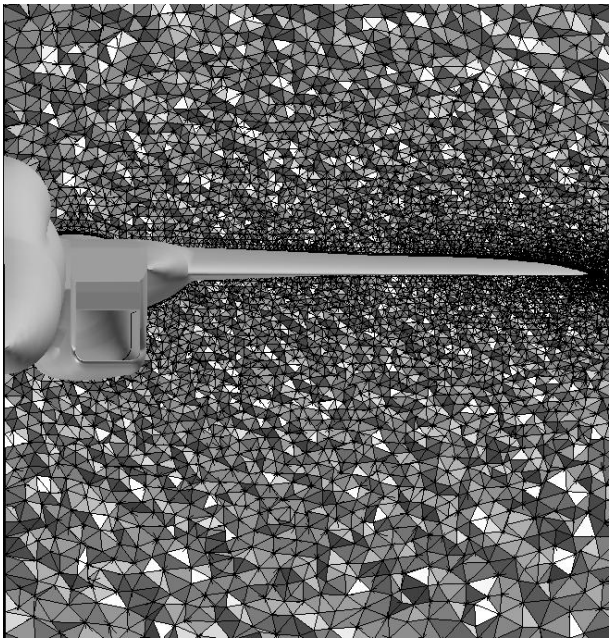

Figure 6: Close up of F-15E grid with a cutting plane across the wing. 5.9 million cell grid, half aircraft.

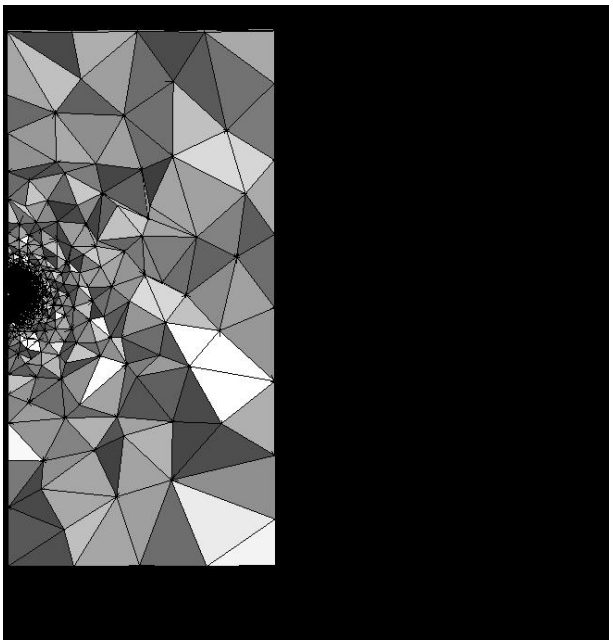

Figure 7: F-15E grid, entire domain.

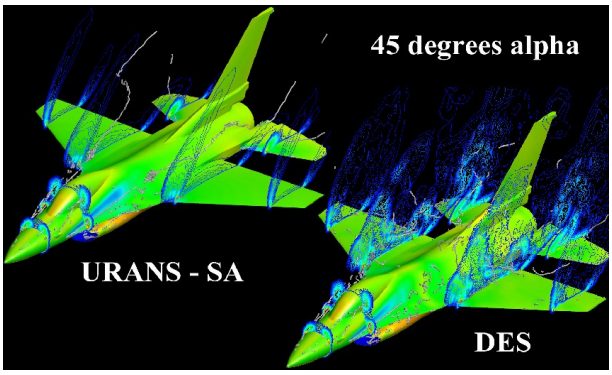

Figure 8: Comparison for the F-16 of RANS (SA) and DES at $\alpha = 45°$. Surface colored by pressure, and contours of vorticity. Gray tubes are auto-detected vortex cores.

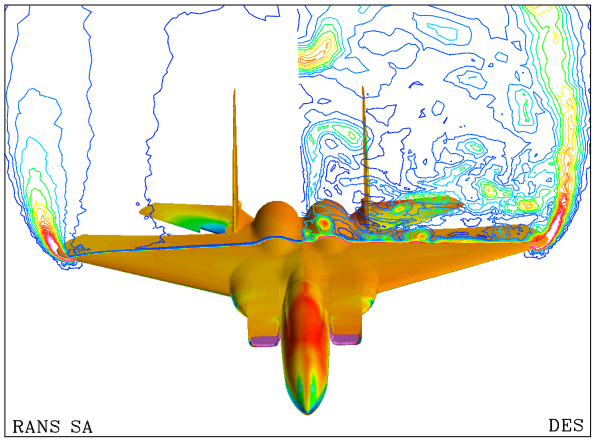

Figure 9: Comparison for the F-15E of RANS (SA) and DES at $\alpha = 65°$. Surface colored by pressure, and contours of vorticity.

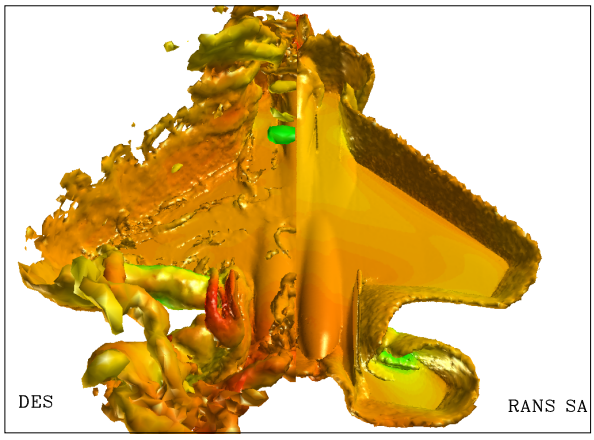

Figure 10: Comparison for the F-15E of RANS (SA) and DES at $\alpha = 65°$. Isosurface of vorticity colored by pressure.

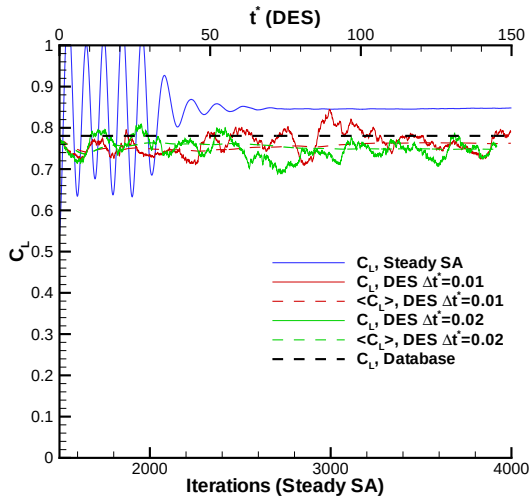

Figure 11: Time and iteration histories of C_L on the F-15E.

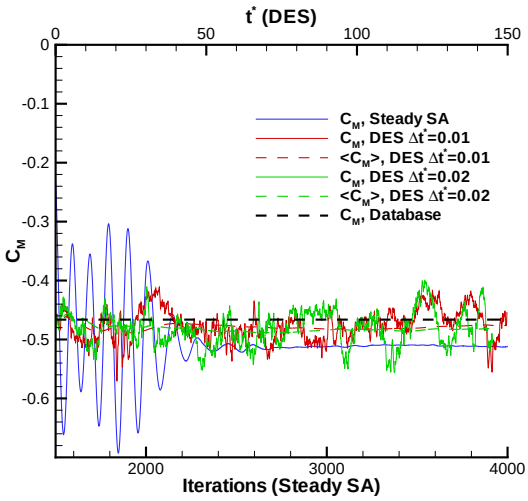

Figure 13: Time and iteration histories of C_M on the F-15E.

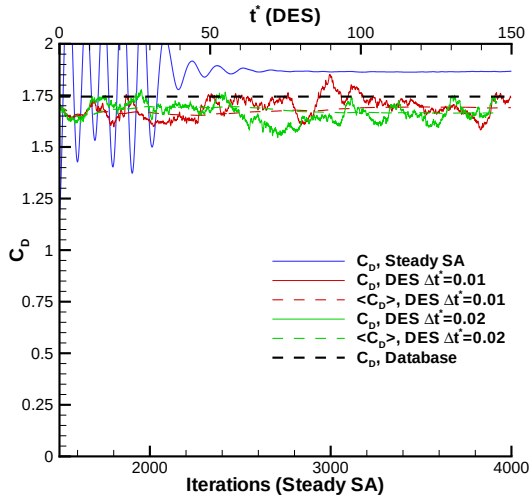

Figure 12: Time and iteration histories of C_D on the F-15E.

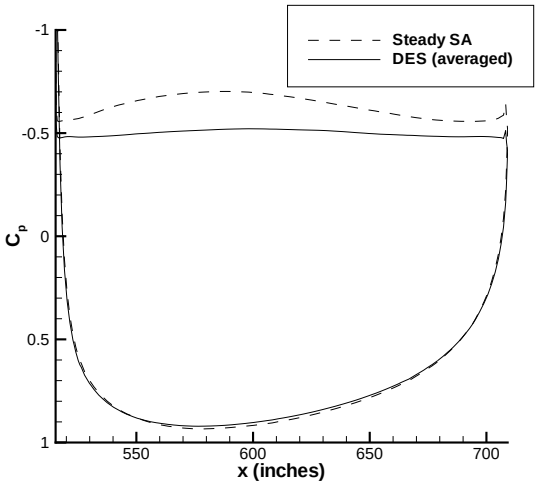

Figure 14: Pressure coefficients on the F-15E wing, 110 inches from centerline - DES (time-averaged) and RANS (SA).